



NRC Publications Archive Archives des publications du CNRC

On the effect of carbon monoxide addition on soot formation in a laminar ethylene/air coflow diffusion flame

Guo, Hongsheng; Thomson, Kevin; Smallwood, Gregory

This publication could be one of several versions: author's original, accepted manuscript or the publisher's version. / La version de cette publication peut être l'une des suivantes : la version prépublication de l'auteur, la version acceptée du manuscrit ou la version de l'éditeur.

For the publisher's version, please access the DOI link below. / Pour consulter la version de l'éditeur, utilisez le lien DOI ci-dessous.

Publisher's version / Version de l'éditeur:

<http://dx.doi.org/10.1016/j.combustflame.2009.01.006>

Combustion and Flame, 156, 6, pp. 1135-1142, 2009

NRC Publications Record / Notice d'Archives des publications de CNRC:

<http://nparc.cisti-icist.nrc-cnrc.gc.ca/npsi/ctrl?action=rtdoc&an=11784566&lang=en>

<http://nparc.cisti-icist.nrc-cnrc.gc.ca/npsi/ctrl?action=rtdoc&an=11784566&lang=fr>

Access and use of this website and the material on it are subject to the Terms and Conditions set forth at

http://nparc.cisti-icist.nrc-cnrc.gc.ca/npsi/jsp/nparc_cp.jsp?lang=en

READ THESE TERMS AND CONDITIONS CAREFULLY BEFORE USING THIS WEBSITE.

L'accès à ce site Web et l'utilisation de son contenu sont assujettis aux conditions présentées dans le site

http://nparc.cisti-icist.nrc-cnrc.gc.ca/npsi/jsp/nparc_cp.jsp?lang=fr

LISEZ CES CONDITIONS ATTENTIVEMENT AVANT D'UTILISER CE SITE WEB.

Contact us / Contactez nous: nparc.cisti@nrc-cnrc.gc.ca.





On the effect of carbon monoxide addition on soot formation in a laminar ethylene/air coflow diffusion flame

Hongsheng Guo*, Kevin A. Thomson, Gregory J. Smallwood

Institute for Chemical Process and Environmental Technology, National Research Council of Canada, 1200 Montreal Road, Ottawa, Ontario, Canada K1A 0R6

ARTICLE INFO

Article history:

Received 9 September 2008
Received in revised form 27 November 2008
Accepted 14 January 2009
Available online 29 January 2009

Keywords:

Soot
Fuel enrichment
Carbon monoxide
Modeling

ABSTRACT

The effect of carbon monoxide addition on soot formation in an ethylene/air diffusion flame is investigated by experiment and detailed numerical simulation. The paper focuses on the chemical effect of carbon monoxide addition by comparing the results of carbon monoxide and nitrogen diluted flames. Both experiment and simulation show that although overall the addition of carbon monoxide monotonically reduces the formation of soot, the chemical effect promotes the formation of soot in an ethylene/air diffusion flame. The further analysis of the details of the numerical result suggests that the chemical effect of carbon monoxide addition may be caused by the modifications to the flame temperature, soot surface growth and oxidation reactions. Flame temperature increases relative to a nitrogen diluted flame, which results in a higher surface growth rate, when carbon monoxide is added. Furthermore, the addition of carbon monoxide increases the concentration of H radical owing to the intensified forward rate of the reaction $\text{CO} + \text{OH} = \text{CO}_2 + \text{H}$ and therefore increases the surface growth reaction rates. The addition of carbon monoxide also slows the oxidation rate of soot because the same reaction $\text{CO} + \text{OH} = \text{CO}_2 + \text{H}$ results in a lower concentration of OH.

Crown Copyright © 2009 Published by Elsevier Inc. on behalf of The Combustion Institute.
All rights reserved.

1. Introduction

Recent development in fuel enrichment combustion and application of syngas stimulates our interest in the effect of carbon monoxide (CO) addition on various flame properties, since CO is a primary component of a reformat gas or a syngas which is an effective and practical enrichment additive [1]. One of these flame properties is soot formation in diffusion flames employing fossil fuels.

Emission of soot not only has a detrimental effect on human health, but also contributes significantly to global warming. Although the effect of the addition of various additives on soot formation has been investigated [2–8], surprisingly there is not much information available in the literature on the effect of CO addition, especially the chemical effect of CO addition, on soot formation. CO contains carbon atom, but is a non-sooting fuel. Therefore, the addition of CO to a hydrocarbon fuel flame has a dilution effect in terms of soot formation. However, CO participates in chemical reactions that may influence soot formation. Consequently, the addition of CO may have complex effect on soot formation. Arthur and Napier [9] noted that the addition of CO had a weakly suppressive effect on soot formation in methane flames, but did not

offer any explanation for the behavior. Du et al. [10] observed that the addition of CO caused a linear decrease in soot formation in an ethylene diffusion flame, and a complicated behavior in a propane diffusion flame. They argued that the addition of CO could chemically promote soot inception chemistry, but did not provide any discussion on the variation in the chemistry of surface growth, another important sub-process of soot formation that contributes most formed soot in terms of the total mass. Therefore, further study is needed to investigate the detailed mechanism of the effect of CO addition on soot formation in diffusion flames.

This paper investigates the effect of CO addition on soot formation in a coflow ethylene/air diffusion flame by both experiment and numerical simulation. Specifically, we are interested in the chemical effect of CO addition on soot formation. To isolate the chemical effect from others, the paper also investigates the addition of nitrogen (N_2), which has similar thermal and dilution effects as CO because they have similar thermal and transport properties. Nitrogen is inert for soot formation and therefore does not have chemical effect. Differently CO has chemical effect since it actively participates in chemical reactions. The chemical effect of CO addition is identified by comparing the results of N_2 and CO diluted flames. The paper starts with the description of experimental methodology, followed by the numerical model. Then the experimental and numerical results are demonstrated and compared, and discussion on the mechanism of the effect of CO addition on soot formation is provided by analyzing the details of numerical data.

* Corresponding author. Fax: +1 613 957 7869.

E-mail address: hongsheng.guo@nrc-cnrc.gc.ca (H. Guo).

2. Experimental methodology

The experiment was conducted in a coflow laminar diffusion flame burner. The fuel stream issued from a 10.9 mm inner diameter vertical tube, and the air from the annular region between the fuel tube and a 88 mm inner diameter concentric tube. The wall thickness of the fuel tube is 0.95 mm. The base flame is a pure ethylene/air diffusion flame. During the experiment, the volume flow rates of air and ethylene were kept the same as in the base flame, i.e. 284 l/min and 194 ml/min (at room temperature and atmospheric pressure condition), respectively, while CO or N₂ was added to the center fuel tube. To keep all the studied flames as attached flames, the investigated volume fraction of CO or N₂ in the fuel stream was limited to less than 0.8. Unless explicitly indicated, in the presentation of this paper, the fraction of CO (α_{CO}) or N₂ (α_{N_2}) in fuel stream is volume based.

The soot volume fraction was measured using the diffuse-light two-dimensional line-of-sight attenuation (LOSA) optical diagnostic method developed by Thomson et al. [11]. The light source for the experiments is a mercury arc lamp diffused by an integrating sphere and imaged to the flame center with a pair of lens doublets. The flame center was imaged by a second pair of lens doublets onto a CCD array filtered with a 450 nm narrow band filter. The magnification of the system is such that each pixel images a square of 23 × 23 μm. The data is binned horizontally and vertically to reduce shot noise and the final spatial resolution is 90 × 500 μm, respectively. A soot refractive index light absorption function, $E(m)_\lambda$, of 0.26 was used in the data analysis [12]. The diagnostic can detect optical thicknesses as low as 0.001 while optical thicknesses in the present measurements were in the order of 0.1. The principal sources of uncertainty in the measurements are bias introduced by light scatter which can be as large as 25% of the measured attenuation and uncertainty in the value of $E(m)_\lambda$. More details of the optical diagnostic method can be found from [11].

3. Numerical model

The above experimental flames were modeled by numerical simulation. The governing equations for conservation of mass, momentum, energy and gas species mass fractions can be found elsewhere [7].

The formation and evolution of soot particles was simulated by the method of moments [13]. The soot particle moments are defined as

$$M_r = \sum_{i=1}^{\infty} m_i^r N_i \quad (1)$$

where M_r is the r th moment of soot particle distribution, and m_i and N_i are the mass and the particle number density, respectively, of the soot particles of size class i . The soot particle mass is represented by the number of carbon atoms. Six concentration moments (i.e. $r = 0, 1, 2, 3, 4, 5$) are used.

The governing equation for each soot concentration moment is

$$\begin{aligned} & \rho u \frac{\partial(M_r/\rho)}{\partial z} + \rho v \frac{\partial(M_r/\rho)}{\partial r} \\ &= \frac{\partial}{\partial z} \left(\rho D_{p,1} \frac{\partial}{\partial z} \left(\frac{M_{r-2/3}}{\rho} \right) \right) + \frac{1}{r} \frac{\partial}{\partial r} \left(r \rho D_{p,1} \frac{\partial}{\partial r} \left(\frac{M_{r-2/3}}{\rho} \right) \right) \\ & \quad - \frac{\partial}{\partial z} (V_{T,z} M_r) - \frac{1}{r} \frac{\partial}{\partial r} (r V_{T,r} M_r) + Q_r \end{aligned} \quad (2)$$

where ρ is density (g/cm³), u and v the axial (z) and radial (r) direction velocities (cm/s), respectively, Q_r the source term, and $M_{r-2/3}$ the fractional moments obtained by interpolation between

the whole moments. Quantity V_{T,x_i} is the thermal diffusion velocity of soot in z or r direction, and is calculated by

$$V_{T,x_i} = -0.55 \frac{\nu}{T} \frac{\partial T}{\partial x_i} \quad (x_i = z \text{ or } r) \quad (3)$$

where ν is the kinematic viscosity. Quantity $D_{p,1}$ is the diffusion rate of the smallest soot particles, and is given by

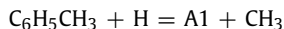
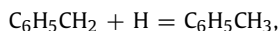
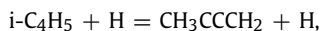
$$D_{p,1} = \frac{3}{2\rho} \sqrt{\frac{\bar{m} k_B T}{2\pi}} \left(1 + \frac{\pi \alpha_T}{8} \right)^{-1} \frac{1}{d_1^2} \quad (4)$$

with \bar{m} being the mean mass of the gas (g), k_B the Boltzmann's constant (erg mol⁻¹ K⁻¹), T the temperature (K), α_T the thermal accommodation coefficient (0.9), and d_1 the diameter of the smallest soot particle (cm). The source term Q_r in each moment equation accounts for particle nucleation, coagulation, surface growth and oxidation of soot particles.

The model assumes that nucleation of soot particles is due to the coalescence of two large size PAH, pyrene (A4), into a dimer. Then the particle size increases or decreases due to the particle coagulation, surface growth and oxidation. The gas phase chemistry and the calculation methods for the particle nucleation, coagulation, surface growth and oxidation are basically those developed by Appel et al. [14] and Frenklach and Wang [13] with some modifications because the original method and chemistry underpredicted soot volume fraction for the diffusion flames of this paper.

The first modification is to the gas phase chemistry. We modified the propargyl (C₃H₃) combination reaction to C₃H₃ + C₃H₃ ⇒ A1- (phenyl) + H, and added the reaction C₃H₃ + C₃H₂ ⇒ A1-, following the suggestion of [15]. The rate constant for the first reaction was raised to 2.E+13 (cm³/mol.s), which resulted in an 18% increase in peak soot volume fraction in the ethylene/air diffusion flame. For the second reaction, the rate constant is the same as in [15].

In addition, more routes and reactions, which have recently been shown to be important in PAH formation and growth by other researchers, were added to the base chemistry [14]. For the formation of benzene (A1), the route of 1-methylallenyl and propargyl combining to form benzyl radicals and their decomposition to benzene [16]



and the reaction C₂H₃ + C₄H₄ = A1 + H [17] were added. Two reaction sequences C₆H₅CH₂ + C₃H₃ = A2 + 2H and C₅H₅ (cyclopentadienyl) + C₅H₅ = A2 + 2H [16] were added to account for the formation of naphthalene (A2). For the formation of phenanthrene (A3), the reaction: Indenyl + C₅H₅ = A3 + 2H [18] was added. The reactions A2-1 + A1 ⇒ A4 + H + H₂, A2-2 + A1 ⇒ A4 + H + H₂, A2 + A1- ⇒ A4 + H + H₂ [19] were added to account for the formation of pyrene (A4). The rate expressions of these added reactions can be found from the corresponding references and their citations. Details of these reactions have been discussed in the references, and will not be repeated. The complete set of gas phase reaction scheme consists of 580 reactions and 108 species.

The second modification is the calculation of coagulation. The free molecular regime was employed. However, we limited the particle coagulation by setting the coagulation rate as zero when the mean particle diameter is greater than 25 nm. This is based on the experimental observation that generally the maximum diameter of a primary particle is about 25–30 nm.

Thirdly, we increased the surface growth rate by raising the parameter α , the fraction of surface sites available for surface reactions. Basically, the parameter α was still calculated by Eq. (1) of [14], i.e.

$$\alpha = \tanh(a/\log \mu_1 + b) \quad (5)$$

where μ_1 is the first size moment of the soot particle distribution. However, the parameter a in the equation was increased by 3 times to $a = 3 \times (12.65 - 5.63 \times 10^{-3} \times T)$, and the parameter b was modified to $b = -1.38 + 1.02 \times 10^{-3} \times T$, with T being local temperature. This modification led to about 44% increase in the peak soot volume fraction for the ethylene/air diffusion flame.

After the above modifications, the peak soot volume fraction of the base flame was reasonably predicted. However, soot volume fraction was still underpredicted in the centerline region, where soot volume fraction calculation is more sensitive to inception rate that is closely related to the concentration of pyrene (the inception species). Realizing that the current gas phase chemistry may still underpredict the concentration of pyrene, we reduced the scrubbing factor of pyrene α_{A4} to 0.03, i.e. the reaction rate of pyrene was calculated by $r_{A4} = r_{g,A4} + \alpha_{A4} \cdot r_{s,A4}$, where r_{A4} , $r_{g,A4}$, $r_{s,A4}$ and α_{A4} are, respectively, the net rate, the rate due to gas phase reactions, the rate due to soot formation and the scrubbing factor of pyrene. This treatment follows a similar idea of Smooke et al. [20], and is an *ad hoc* one. However, it should not affect the primary conclusion of this paper, since we focus on the relative variation, when CO or N₂ is added. The scrubbing factors for all other species are unity.

The above modification and addition of gas phase reactions and the reduction of the scrubbing factor of pyrene led to more significant improvement in the prediction of centerline region soot volume fraction than that of peak soot volume fraction. Without the modification and addition of the mentioned reactions for PAH formation and growth, the scrubbing factor of pyrene would have to be reduced to 5.E–04 for the ethylene/air diffusion flame to obtain relatively reasonable soot volume fraction in centerline region. On the other hand, the prediction of peak soot volume fraction, which is located in an annular flame wing region (see results later), is more sensitive to the modification in the parameter α (Eq. (5)) that changes the surface growth rate. A sole increase in the parameter α and thus the surface growth rate was never successful to improve the underprediction of centerline region soot volume fraction, even if it was increased to an unreasonable value (greater than unity) and the peak soot volume fraction was significantly overpredicted.

Low Mach number assumption was adopted. The governing equations were discretized using the finite volume method in axisymmetric cylindrical coordinates. The SIMPLE numerical scheme [21] was used to handle the pressure and velocity coupling. The diffusion terms in the conservation equations were discretized by the central difference method and the convective terms were discretized by the power law method [21]. To speed up the convergent process, the discretized governing equations of gas species and soot moments were, respectively, solved in a fully coupled fashion at each control volume [22]. Those of momentum, energy and pressure correction were solved using the tri-diagonal matrix algorithm.

The computational domain covers an area from 0 to 3.0 cm in the radial (r) direction and 0 to 11.0 cm in the axial (z) direction. The inflow boundary ($z = 0$ cm) corresponds to the region immediately above the fuel nozzle. Totally 160 (z) \times 95 (r) non-uniform grids were used in the simulations, with finer grids placed in the primary reaction zone and near the fuel nozzle exit region. It has been checked that the further increase of grid number does not significantly influence the simulation results. The thermal and

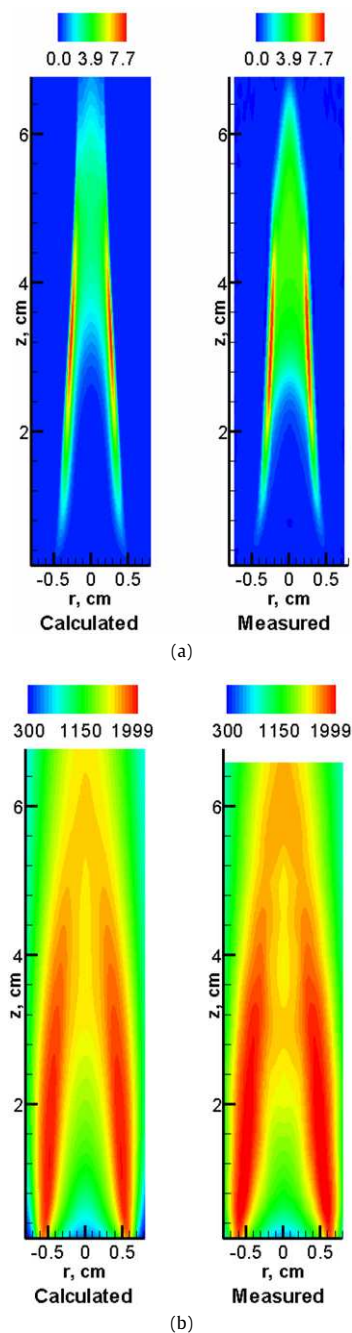


Fig. 1. Calculated and measured soot volume fraction (ppm) and flame temperature (K) for the pure C₂H₄/air flame. (a) Soot volume fraction; (b) temperature.

transport properties were obtained by using the algorithms given in [23,24], respectively.

Radiation heat transfer was calculated by the method given by Liu et al. [25]. Other details of the numerical methods can be found from our previous publications [7,26].

4. Results and discussion

Fig. 1 displays the calculated and measured soot volume fraction and flame temperature distributions for the base flame, i.e. the pure ethylene/air flame. The measured temperature data in Fig. 1 is taken from those obtained previously in our laboratory by CARS system [4]. It is observed that although soot volume fraction in the lower centerline region is slightly underpredicted, the simulation has captured the primary features of soot and temperature field.

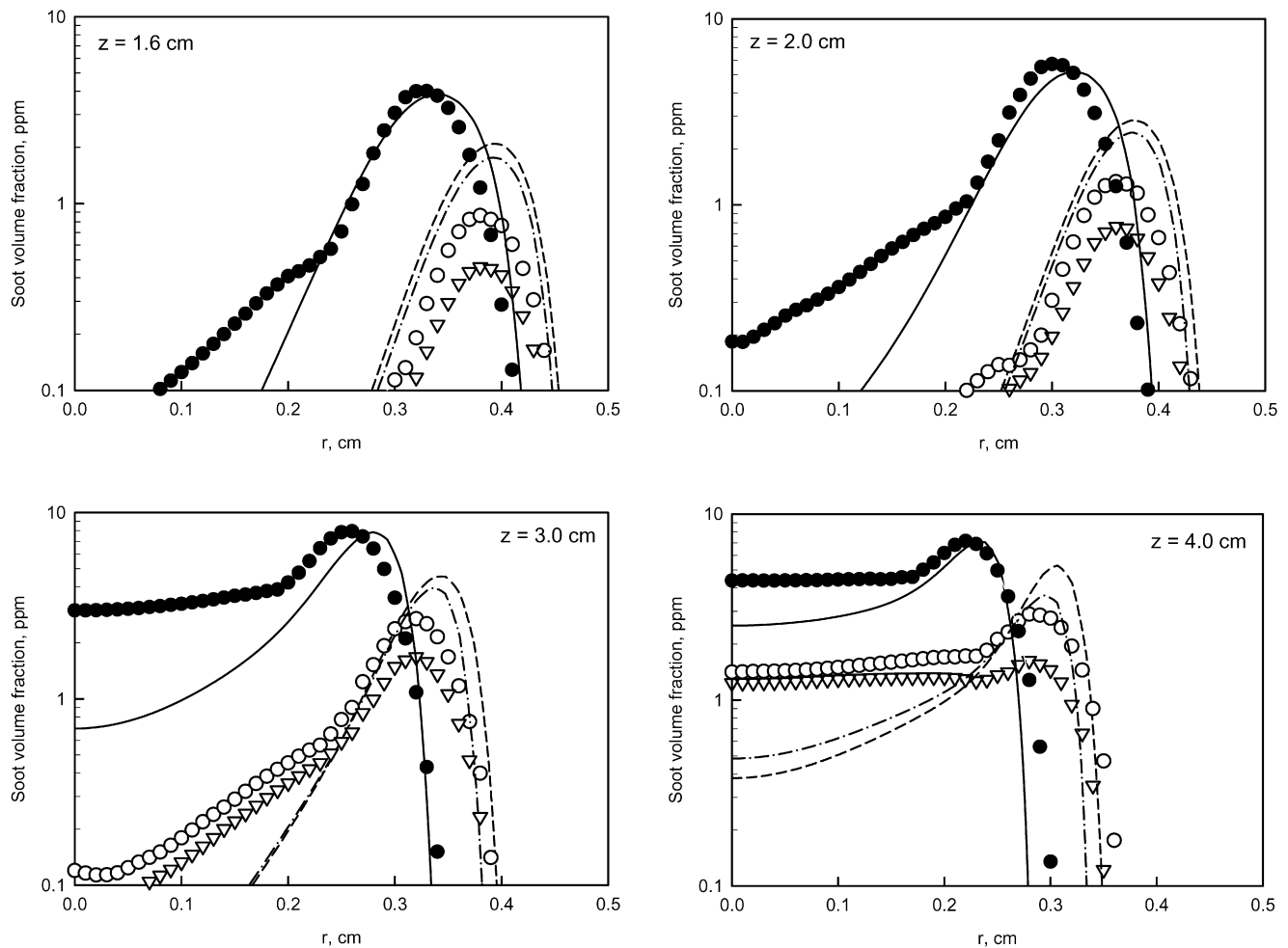


Fig. 2. Radial profiles of soot volume fraction at four different sections above burner exit for pure C_2H_4 /air flame, 60% CO diluted flame and 60% N_2 diluted flame. Pure C_2H_4 /air flame: (—) calculated, (●) measured; 60% CO diluted flame: (---) calculated, (○) measured; 60% N_2 diluted flame: (- · - ·) calculated, (▽) measured.

The peak soot volume fraction calculated is almost the same as the measured. The distributions of soot volume fraction and flame temperature are also reasonably predicted. The slight underprediction of soot volume fraction in the lower centerline region may be due to the preheating effect of fuel stream by nozzle which was not taken into account in the model of this paper. The peak flame temperature is underpredicted by about 3% (73 K). This is an acceptable error.

Fig. 2 shows the radial profiles of soot volume fraction at four axial heights above burner exit for the base ethylene/air flame and flames with 60% CO ($\alpha_{CO} = 0.6$) and 60% N_2 ($\alpha_{N_2} = 0.6$), respectively, in the fuel stream. The selected four axial heights cover the primary soot formation regions. The simulation overpredicted soot volume fractions for the CO and N_2 diluted flames, suggesting that there is a need to further improve soot chemistry and model in the future. However, it captured the relative differences among the three flames.

The integrated soot volume fractions for the three flames are illustrated in Fig. 3. The integrated soot volume fraction was obtained by

$$F_v = \int 2\pi r f_v dr \quad (6)$$

where f_v is the local soot volume fraction. We observe that the simulation underpredicted the maximum integrated soot volume fraction, but again captured the primary phenomena of the experiment. The underprediction of the maximum integrated soot

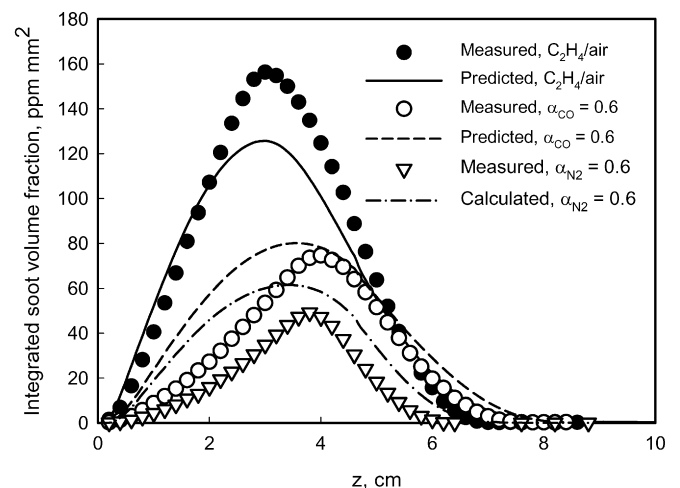


Fig. 3. Integrated soot volume fraction (ppm mm^2).

volume fraction is due to the lower soot volume fraction in the lower centerline region from simulation, as in Figs. 1 and 2.

Figs. 2 and 3 show that soot volume fractions in the 60% CO and 60% N_2 diluted flames are lower than in the base flame, and that in the CO diluted flame is higher than in the N_2 diluted flame. Flames with other fractions of CO or N_2 in the fuel stream have similar phenomena, which can be shown by the variation of the normal-

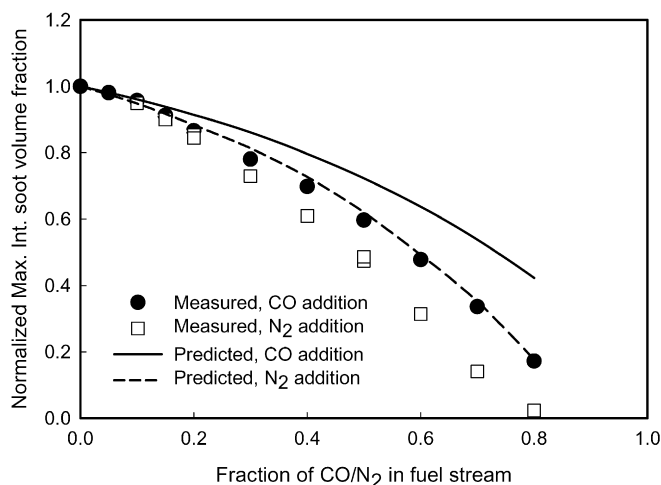


Fig. 4. Normalized maximum integrated soot volume fraction.

ized maximum integrated soot volume fraction ($F_{v,max}/F_{v,max,base}$) versus the fraction of CO/N₂ in the fuel stream, with $F_{v,max}$ being the maximum integrated soot volume fraction of a diluted flame, and $F_{v,max,base}$ being that of the base flame, as in Fig. 4. It reveals that the addition of either CO or N₂ monotonically reduces the formation of soot in the ethylene/air diffusion flame. This is consistent with the study of Du et al. [10]. Moreover, Fig. 4 illustrates that the addition of N₂ is more effective than that of CO in suppressing soot formation at all diluent fractions.

As for other gaseous additives, the addition of CO or N₂ suppresses soot formation by the thermal, dilution and chemical effects. Since CO and N₂ have similar thermal and transport properties, the addition of them has similar thermal and dilution effects. However, N₂ is basically inert for soot formation [27] while CO actively participates in chemical reactions. Therefore, the difference between the CO and N₂ diluted flames reflects the chemical effect of CO addition. Accordingly, Figs. 2–4 imply that the chemical effect of CO addition actually promotes the formation of soot in an ethylene/air diffusion flame. This is opposite to the chemical effect of hydrogen or carbon dioxide addition on soot formation [4,7,28].

There has been extensive discussion on the thermal and dilution effects on soot formation in a diffusion flame, such as [5] and the citations therein. Therefore, we focus on the chemical effect of CO addition in this paper. We do this by comparing the numerical details of CO and N₂ diluted flames below, taking the 60% CO and 60% N₂ flames as examples, since the numerical model has successfully captured the relative difference between CO and N₂ diluted flames for this and other diluent fractions.

Soot formation consists of three sub-processes: inception, surface growth and oxidation. We first check inception. Fig. 5 displays radial profile of the inception rate for the 60% CO and 60% N₂ diluted flames at the four axial heights, which correspond to those in Fig. 2. It shows that inception rate in the CO diluted flame is lower than in the N₂ diluted flame. This is opposite to the relative difference in soot volume fractions in the CO and N₂ diluted flames. Therefore, the chemical effect of CO addition, which promotes the formation of soot, is not through inception. A reaction pathway analysis indicates that the lower inception rate in the CO diluted flame results from the reaction $C_2H_4 + C_2H_3 = C_4H_6 + H$. The fuel pyrolysis rate is higher due to higher temperature, as shown later, which causes the lower concentration of C₂H₄ and finally the lower formation rate of C₄H₆ in the CO diluted flame. The lower formation rate of C₄H₆ results in the slower formation rate of inception species, pyrene (A4), and thus the lower inception rate in the CO diluted flame, due to the reaction sequence $C_2H_3 + C_4H_6 = CH_3 + C_5H_6$, $C_5H_6 + H = C_5H_5 + H_2$, $C_5H_5 + C_5H_5 = A2 + 2H$,

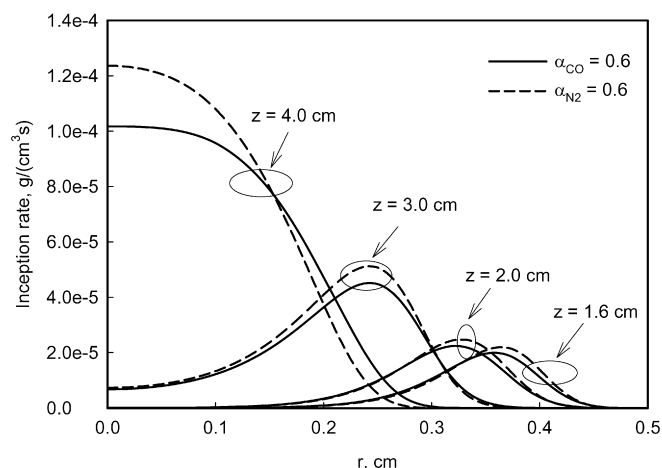


Fig. 5. Particle inception rate.

and $A2 \Rightarrow A3 \Rightarrow A4$. However, we note that this numerical result of the lower inception rate in the CO diluted flame is not consistent with the observation of Du et al. [10] on soot inception limit. Although we are not sure if the inception limit exactly reflects inception chemistry, the effect of CO addition on particle inception and the role of the above reaction sequence for PAH formation may need further study in the future.

Surface growth rate equals the product of specific surface growth rate (growth rate per unit surface area, g/cm² s) and specific surface area (surface area per unit volume, cm⁻¹). Please note that here surface growth does not include oxidation, which will be discussed later separately. The radial profiles of specific surface area, specific surface growth rate and particle number density in the two flames are shown in Fig. 6. It is noted that both the specific surface area and specific surface growth rate of the CO diluted flame are higher than those of the N₂ diluted flame. Therefore, the surface growth rate of the CO diluted flame is higher than that of the N₂ diluted flame, meaning that surface growth is one sub-process through which the addition of CO chemically promotes soot formation. It should be pointed out that the bigger specific surface area of the CO diluted flame is also caused by the higher specific surface growth rate, since the particle number density of the CO diluted flame is actually lower than that of the N₂ diluted flame, as shown in Fig. 6c, due to the lower inception rate (Fig. 5). The higher specific surface growth rate results in larger particle size and thus the bigger specific surface area in the CO diluted flame than in the N₂ diluted flame. Therefore, we can analyze the surface growth reactions to identify how the addition of CO chemically promotes soot formation.

Surface growth includes PAH condensation and acetylene (C₂H₂) addition. However, the simulation indicates that C₂H₂ addition dominates, and the higher specific surface growth rate in the CO diluted flame is primarily because of C₂H₂ addition. Therefore, we will examine how the addition of CO chemically affects C₂H₂ addition. In the numerical model, the rate of C₂H₂ addition is calculated by the mechanism of H-abstraction-carbon-addition (HACA) [13,14], in which the two key reactions are $C_{soot}-H + H = C_{soot}\cdot + H_2$ (formation of active site by H-abstraction) and $C_{soot}\cdot + C_2H_2 \Rightarrow C_{soot}-H + H$ (carbon-addition reaction). This suggests that the primary factors affecting the rate of C₂H₂ addition include temperature and concentrations of C₂H₂ and H radical.

Fig. 7 displays the temperature distributions at the four axial heights. Although not shown, the simulation shows that the peak temperatures of the ethylene/air flame and the 60% CO diluted flame are almost same (about 2063 K), although the adiabatic temperatures of the two flames are not exactly same. This is due to

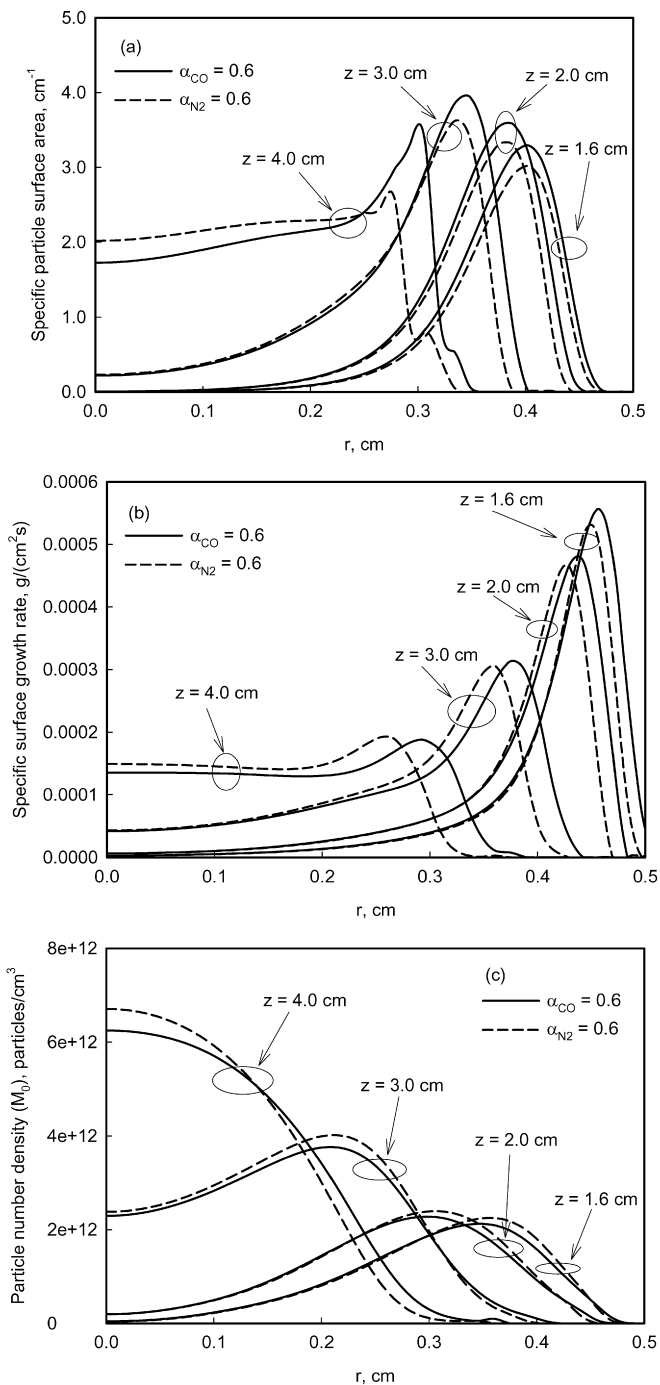


Fig. 6. Radial profiles of specific surface area, specific surface growth rate and particle number density. (a) Specific surface area; (b) specific surface growth rate; (c) particle number density.

the difference in radiation heat loss caused by soot. The peak temperature of the 60% N_2 diluted flame is 1971 K, even though it has the lowest soot volume fraction among the three flames. Temperature in the CO diluted flame is higher than in the N_2 diluted flame, which tends to increase the rate of C_2H_2 addition. This is as expected, since CO actively participates in chemical reactions and releases heat, while N_2 does not. Therefore, the higher temperature is a factor that causes the higher surface growth rate in the CO diluted flame. Since the higher temperature in the CO diluted flame, relative to the N_2 diluted flame, is caused by CO's participating in chemical reactions, we attribute this factor as a chemical effect.

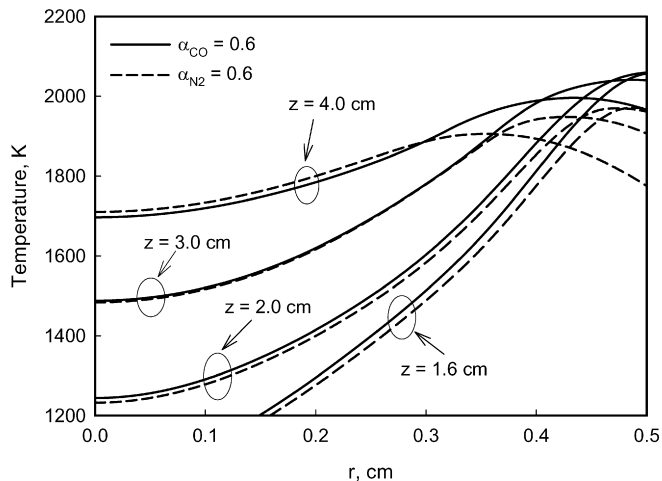


Fig. 7. Flame temperature distribution.

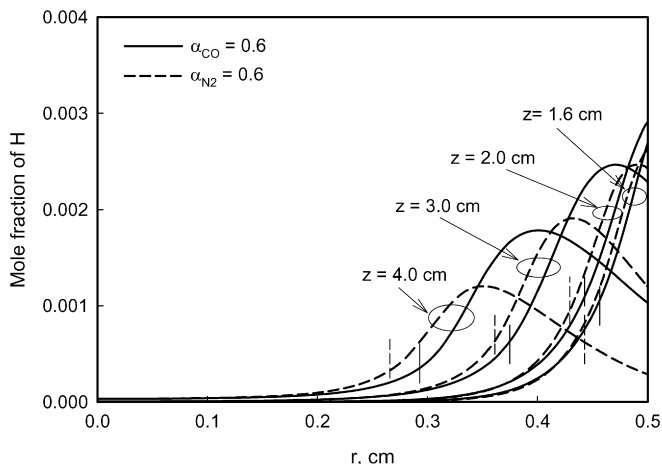


Fig. 8. Concentration of H radical. Short vertical lines indicate the peak specific surface growth rate positions, with solid being for the CO diluted flame and dashed for the N_2 diluted flame.

The second factor that may influence the rate of C_2H_2 addition is the concentration of H radical, which controls the formation rate of active site [13,14] for C_2H_2 addition. The radial profiles of H radical at the four axial heights are shown in Fig. 8, where the short vertical line (solid for CO diluted flame and dashed for N_2 diluted flame) on each curve indicates the positions where surface growth rate reaches its peak value at the corresponding axial height. We note that overall the concentration of H radical is higher in the CO diluted flame than in the N_2 diluted flame. This is because of the reaction $CO + OH = CO_2 + H$, whose forward rate is increased when CO is added. The higher concentration of H radical results in the higher active site formation ($C_{soot} + H = C_{soot}^* + H_2$) rate and finally the higher surface growth rate in the CO diluted flame as compared to the N_2 diluted flame. This suggests that the higher concentration of H radical may be another factor that causes the chemical effect of CO addition that promotes soot formation. However, we also note that the difference in the concentrations of H radical of the two flames in the peak surface growth regions become negligible at $z = 3.0$ and 4.0 cm. Accordingly, this fact may be only important in the lower flame region.

The last factor that may affect the rate of C_2H_2 addition is the concentration of C_2H_2 , as shown in Fig. 9. Overall, the concentration of C_2H_2 is higher in the CO diluted flame than in the N_2 diluted flame. It is because of the reaction $C_2H_2 + O = CO + CH_2$,

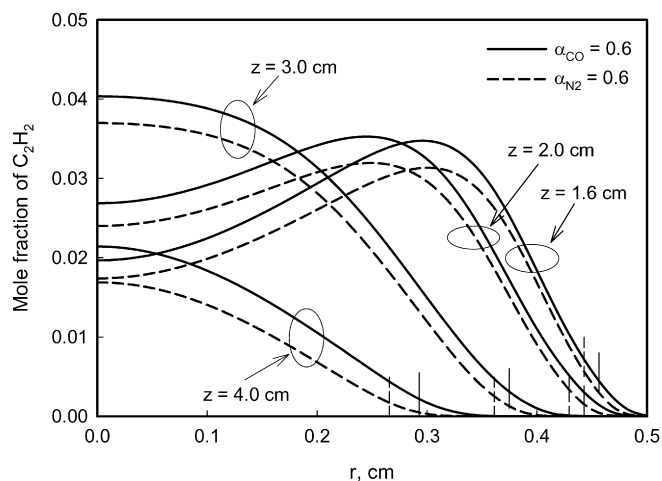


Fig. 9. Concentration of acetylene (C_2H_2). Short vertical lines indicate the peak specific surface growth rate positions, with solid being for the CO diluted flame and dashed for the N_2 diluted flame.

which is the primary destruction reaction of C_2H_2 . When CO is added, the reverse rate of this reaction is intensified, resulting in the lower C_2H_2 destruction rate and thus higher concentration of C_2H_2 . However, since the peak surface growth rate positions (indicated by the short vertical lines, with solid being for CO diluted flame and dashed for N_2 diluted flame) of the two flames differ, as in Fig. 6b, we note that the concentration of C_2H_2 in the peak surface growth region at $z = 1.6$ and 2.0 cm is actually lower in the CO diluted flame than in the N_2 diluted flame. In the upper flame region, the difference in C_2H_2 between the two flames in the peak surface growth region is negligible. Consequently, C_2H_2 may not be a factor that results in the higher surface growth rate due to the chemical effect of CO addition. Therefore, the simulation result of this paper suggests that the chemical effect of CO addition on surface growth rate could be due to the higher temperature and faster formation rate of H radical.

Now we examine how the addition of CO influences soot oxidation. Being consistent with the current understanding in the literature, the simulation indicates that the oxidation of soot is primarily due to the attack of OH on soot particles. Fig. 10 displays the concentration of OH at the four axial heights. It is observed that the concentration of OH radical in the near centerline region, where soot exists (as shown in Fig. 2), is lower in the CO diluted flame than in the N_2 diluted flame. As with the H radical, this is also due to the reaction $CO + OH = CO_2 + H$, which intensifies the consumption rate of OH when CO is added. The lower concentration of OH tends to slow the oxidation rate of soot in the CO diluted flame and to increase the net soot formation rate. This may be another factor that causes the chemical effect of CO addition on soot formation. This is similar to the suggestion of Du et al. [10], and consistent with the viewpoint of Puri and Santoro [29] who indicated that soot and CO oxidation competed each other for OH.

In summary, the above discussion suggests that the chemical effect of CO addition that promotes the formation of soot in the ethylene/air diffusion flame may be primarily a temperature increase, resulting from chemical reactions, and the modifications in the reaction $OH + CO = CO_2 + H$ which lowers the concentration of OH, and increases the concentration of H. The higher concentration of H intensifies soot surface growth rate, and the lower concentration of OH slows the oxidation rate of OH, when CO is added.

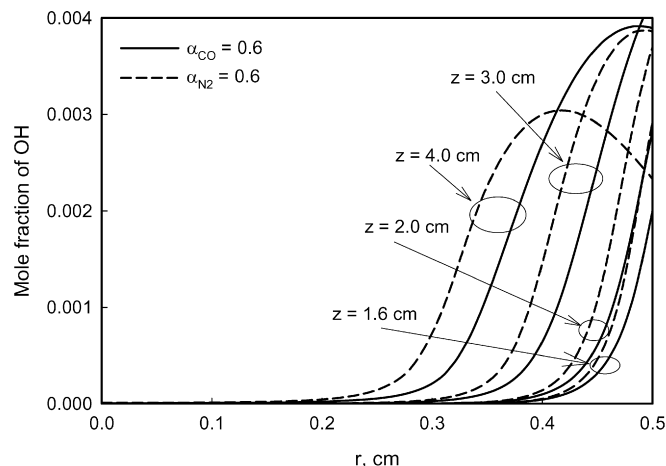


Fig. 10. Concentration of OH.

5. Conclusions

An experimental and numerical study has been conducted on the effect of CO addition on soot formation in an ethylene/air diffusion flame, with special emphasis on the chemical effect. The chemical effect is isolated from the thermal and dilution effects by comparing the results of CO and N_2 diluted flames. Both experiment and simulation show that the addition of both CO and N_2 monotonically reduces the formation of soot. However, the addition of N_2 is more effective than that of CO in suppressing soot formation, implying that the addition of CO chemically promotes the formation of soot, which is different from the chemical effect of carbon dioxide or hydrogen addition. The further analysis of the details from numerical simulation suggests that the chemical effect of CO addition that promotes the formation of soot could be due to three factors. (1) Compared to the addition of N_2 , the addition of CO takes part in heat release process and results in higher flame temperature. This causes the higher surface growth rate in the CO diluted flame than in the N_2 diluted flame. (2) When CO is added, the concentration of H radical is increased due to the intensified forward rate of the reaction $OH + CO = CO_2 + H$, which results in the higher surface growth rate for soot formation. (3) Due to the same reaction, the addition of CO reduces the concentration of OH radical and consequently slows the oxidation rates of soot. These three factors cause the chemical effect of CO addition that promotes the formation of soot.

Acknowledgments

We would like to thank Mr. M.F. Baksh for conducting the experiment, and to thank Ms. C. Yang for helping to prepare experiment. The financial support of the Government of Canada's PERD/AFTER program is also acknowledged.

References

- [1] H. Guo, G.J. Smallwood, Ö.L. Gülder, Proc. Combust. Inst. 31 (2007) 1197–1204.
- [2] K.P. Schug, Y. Manheimer-Timnat, P. Yaccarino, I. Glassman, Combust. Sci. Technol. 22 (1980) 235–250.
- [3] D.X. Du, R.L. Axelbaum, C.K. Law, Proc. Combust. Inst. 23 (1990) 1501–1507.
- [4] Ö.L. Gülder, D.R. Snelling, R.A. Sawchuk, Proc. Combust. Inst. 26 (1996) 2351–2358.
- [5] I. Glassman, Proc. Combust. Inst. 27 (1998) 1589–1596.
- [6] H. Guo, F. Liu, G.J. Smallwood, Ö.L. Gülder, Proc. Combust. Inst. 29 (2002) 2359–2365.
- [7] H. Guo, F. Liu, G.J. Smallwood, Ö.L. Gülder, Combust. Flame 145 (2006) 324–338.
- [8] P. Pandey, B.P. Pundir, P.K. Panigrahi, Combust. Flame 148 (2007) 249–262.
- [9] J.R. Arthur, D.H. Napier, Proc. Combust. Inst. 5 (1955) 303–316.

- [10] D.X. Du, R.L. Axelbaum, C.K. Law, *Combust. Flame* 102 (1995) 11–20.
- [11] K.A. Thomson, M.J. Johnson, D.R. Snelling, G.J. Smallwood, *Appl. Opt.* 47 (2008) 694–703.
- [12] D.R. Snelling, K.A. Thomson, G.J. Smallwood, Ö.L. Gülder, *Appl. Opt.* 38 (1999) 2478–2485.
- [13] M. Frenklach, H. Wang, in: H. Bockhorn (Ed.), *Soot Formation in Combustion: Mechanisms and Models*, vol. 59, Springer-Verlag, Berlin, 1994, pp. 162–196.
- [14] J. Appel, H. Bockhorn, M. Frenklach, *Combust. Flame* 121 (2000) 122–136.
- [15] A. D'Anna, A. D'Alessio, *Combust. Flame* 125 (2001) 1196–1206.
- [16] A. D'Anna, J.H. Kent, *Combust. Flame* 144 (2006) 249–260.
- [17] P. Lindstedt, G. Skevis, *Proc. Combust. Inst.* 26 (1996) 703–709.
- [18] N.M. Marinov, W.J. Pitz, C.K. Westbrook, M.J. Castaldi, S.M. Senhan, *Combust. Sci. Technol.* 116–117 (1996) 211–287.
- [19] M.B. Colket, D.J. Seery, *Proc. Combust. Inst.* 25 (1994) 883–891.
- [20] M.D. Smooke, M.B. Long, B.C. Connelly, M.B. Colket, R.J. Hall, *Combust. Flame* 143 (2005) 613–628.
- [21] S.V. Patankar, *Numerical Heat Transfer and Fluid Flow*, Hemisphere, New York, 1980.
- [22] Z. Liu, C. Liao, C. Liu, S. McCormick, in: 33rd Aerospace Science Meeting and Exhibit, Reno, NV, January 9–12, 1995, AIAA paper 95-0205.
- [23] R.J. Kee, J.A. Miller, T.H. Jefferson, Sandia Report SAND 80-8003, Sandia National Laboratories, 1980.
- [24] R.J. Kee, G. Dixon-Lewis, J. Warnatz, M.E. Coltrin, J.A. Miller, Report No. SAND 86-8246, Sandia National Laboratories, 1986.
- [25] F. Liu, H. Guo, G.J. Smallwood, Ö.L. Gülder, *Combust. Flame* 138 (2004) 136–154.
- [26] H. Guo, F. Liu, G.J. Smallwood, Ö.L. Gülder, *Combust. Theory Modelling* 6 (2002) 173–187.
- [27] H. Guo, G.J. Smallwood, *Combust. Flame* 149 (2007) 225–233.
- [28] H. Guo, G.J. Smallwood, *Combust. Sci. Technol.* 180 (2008) 1695–1708.
- [29] R. Puri, R.J. Santoro, *Combust. Flame* 97 (1994) 125–144.